

# Design Methodology for Sievenpiper High-Impedance Surfaces: An Artificial Magnetic Conductor for Positive Gain Electrically Small Antennas

Sergio Clavijo, Rodolfo E. Díaz, and William E. McKinzie, III

**Abstract**—The Sievenpiper high-impedance surface is a periodic structure characterized by a substrate filled with an array of vertical vias, capped by a capacitive frequency selective surface (FSS). It functions as the ideal antenna groundplane for wireless applications because it simultaneously enhances the gain of the antenna as it suppresses the surface waves associated with it (thus reducing the undesired back-lobe and the reactive coupling to nearby circuits). These two properties are known to occur approximately over the frequency bandwidth where the phase of the reflection coefficient of the surface changes from  $+90^\circ$  to  $-90^\circ$ . Since this behavior takes place at frequencies where the unit cell of the structure is small compared to the wavelength, it can be modeled in terms of a layered homogeneous material where each layer has an anisotropic magneto-dielectric tensor. These tensors, readily derived using an effective medium model, can be designed to obtain independent control of the bandwidths of gain increase and surface wave suppression. Based on a transverse resonance model of the effective medium material model, it is shown that Sievenpiper high-impedance surfaces exist that can suppress TE surface waves alone or TM surface waves alone, or both TE and TM surface waves at the same time. Maximum TM surface wave suppression bandwidth is obtained when the distance between the vias in the via array is as close as possible to  $\lambda/2$ . Maximum TE bandwidth is obtained when the conductors of the capacitive FSS offer maximum blockage to the normal magnetic field of the wave. A reduction of the transverse resonance solution to nearly closed form is used to obtain a simple picture of the design space available when the desired operating frequency is fixed.

**Index Terms**—Antennas, artificial magnetic conductors, electromagnetic bandgap, metamaterials, surface waves.

## I. INTRODUCTION

THE WIDESPREAD use of wireless devices, together with the requirement to fit them in ever smaller packages, places radiating antennas in close proximity to sensitive electronic and biological systems. As a result the antenna design faces the competing requirements of maximum radiated gain

Manuscript received October 3, 2002; revised May 23, 2003. The work presented here is a continuation of the work performed with Titan Aerospace in their ARCHES program, managed by V. Sanchez, sponsored by the Defense Advanced Research Projects Agency (DARPA) under Contract F19628-99-C-0080, managed by AFRL/SNHA, Hanscom AFB, MA. RECAP agents: J. Turtle and L. Poles.

S. A. Clavijo and R. E. Díaz are with the Department of Electrical Engineering, Arizona State University, Tempe, AZ 85287 USA (sergio.clavijo@asu.edu; rudydiaz@asu.edu).

W. E. McKinzie is with Etenna Corporation, Laurel, MD 20707 USA (wmckinzie@etenna.com).

Digital Object Identifier 10.1109/TAP.2003.817575

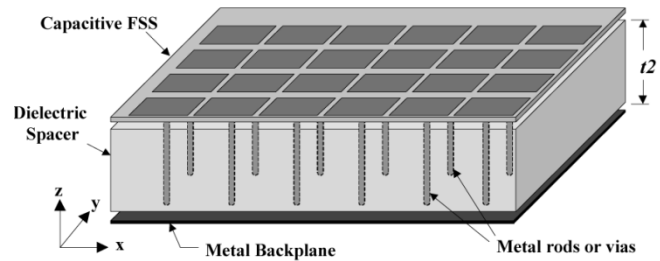


Fig. 1. Sketch of the typical Sievenpiper structure.

with minimized near-field coupling to the environment. The Sievenpiper high-impedance surface [1] is the ideal solution to this problem. It is an electrically thin in-phase reflector with surface wave suppression. Even though it is electrically thin, its surface presents a high impedance within a given frequency band such that the image currents due to a low profile horizontal antenna are in phase with the currents of the antenna itself, instead of  $180^\circ$  out of phase as with conventional metallic ground planes. Furthermore since over the same band it suppresses surface waves, no power is lost into the dielectric as in conventional patch antennas. These two properties result in a net increase in efficiency.

The high-impedance structure is composed of a bed of nails (via array) embedded in a dielectric substrate with a capacitive frequency selective surface (FSS) layer on the top. The FSS can vary in shape but is essentially a two-dimensional (2-D) sheet of disconnected metal obstacles. Fig. 1 shows the physical aspect of the structure with an FSS made of square metal patches. We will use the same Cartesian coordinates shown in Fig. 1 in the rest of the paper.

This structure is not an electromagnetic band gap (EBG) material in the traditional sense because it does not derive its surface wave suppression properties from Bragg scattering between the waves and its periodic unit cell. In fact, it typically operates at frequencies where the period is a small fraction of the wavelength, typically  $\lambda_0/40$  to  $\lambda_0/20$  where  $\lambda_0$  is a free space wavelength at the high impedance resonance. Therefore the structure can be viewed instead as an artificial anisotropic magneto-dielectric material operating below its first periodic structure (Bragg) resonance. It exhibits a frequency-dependent negative permittivity as well as permeability smaller than unity providing in that way a very peculiar medium for the propagation of electromagnetic waves. So-called left-handed

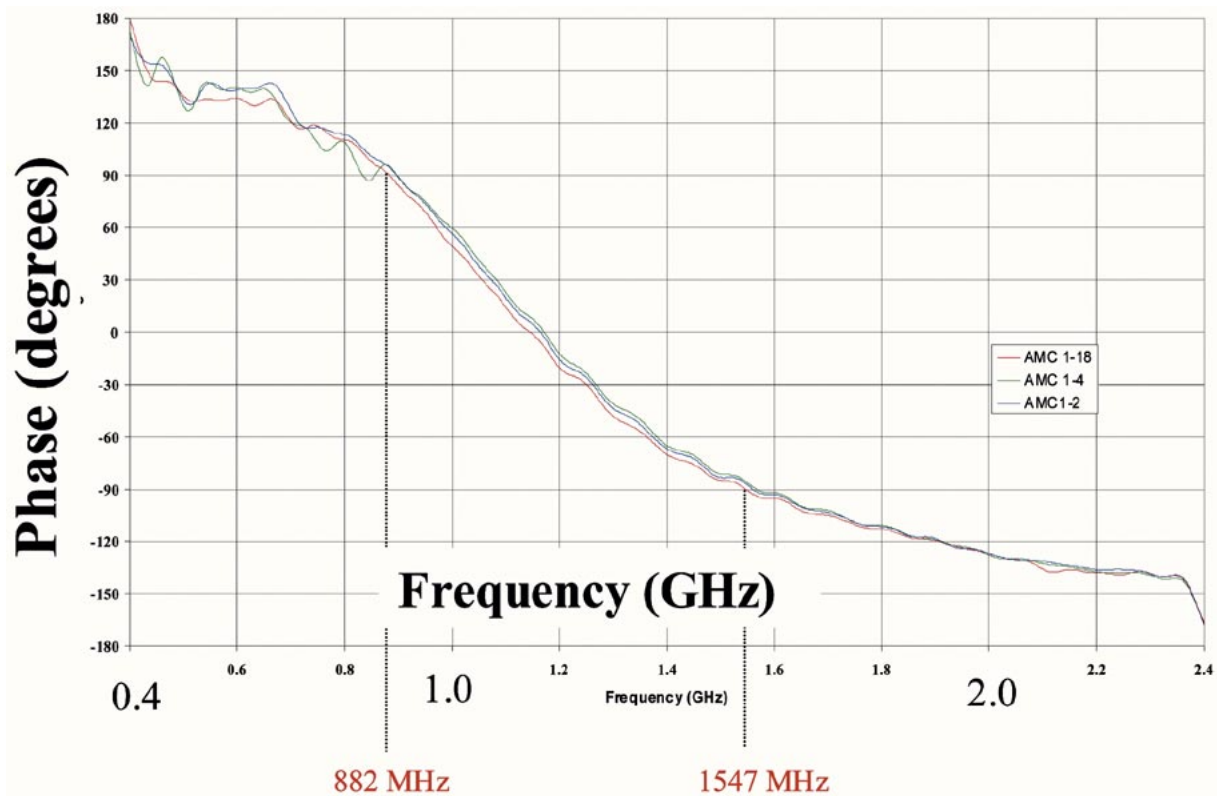


Fig. 2. Measured phase of the reflection coefficient of a high impedance surface 30.5-mm thick, with an operational bandwidth from 0.88 to 1.55 GHz.

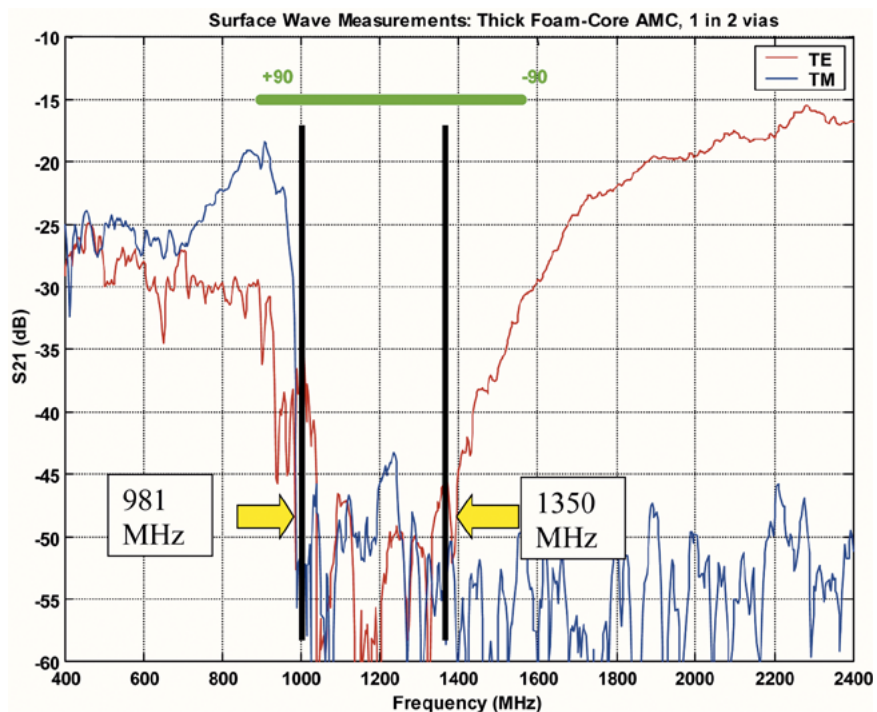


Fig. 3. Measured surface wave transmission coefficient for the high impedance surface of Fig. 2, showing the surface wave suppression bandgap from 0.98 to 1.35 GHz.

or double negative materials make use of similar principles to obtain negative permittivities [2], [3].

The fact that these properties are obtained from a periodic arrangement of elements should not be construed to mean that the periodicity is essential to obtaining the desired values

of the constitutive parameters. As is well known in effective medium theory, given a desired average (homogenized) constitutive property to be obtained from a binary mixture, the periodic arrangement of inclusions (elements) is simply the easiest configuration to analyze, whereas the random mixture

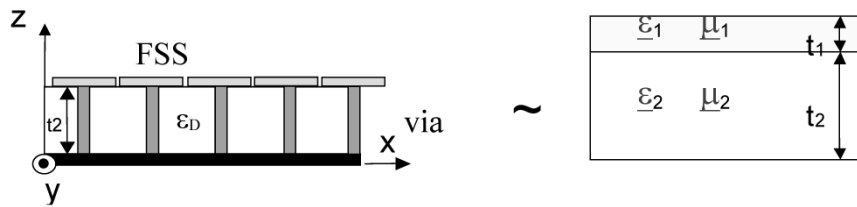


Fig. 4. Side view of the structure and its equivalent two-layer medium.

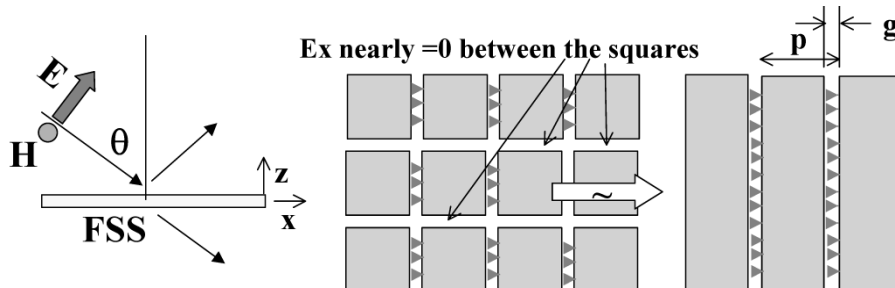


Fig. 5. FSS in the presence of a TM wave reduces to the case of TM incidence onto a parallel strip array.

is usually the easiest configuration to manufacture [4]. That the two attain the same average values in the limit where the average distance between inclusions is small compared to the wavelength has been well established [5]. It is true, however, that as the wavelength of concern approaches the average spacing between inclusions, the low frequency homogenization approximation breaks down. When this breakdown occurs in a periodic medium we have the onset of periodic or Bragg-like scattering effects. When it occurs in a disordered medium we have the onset of multiple-scatterer diffusion (which gives rise for instance to the opacity of fog).

The organization of this paper is as follows. In Section II, a two-layer effective medium model is derived for the high-impedance surface. In Section III, this model is applied with the transverse resonance procedure to determine the propagation constant of the surface waves guided by the structure. It is shown that the surface wave suppression properties are a result of the unusual axial constitutive properties of the material and that the location of the band edges of surface-wave suppression need not be correlated to the  $+90^\circ$  and  $-90^\circ$  phase shift points of the reflection coefficient. In Section IV the physical parameters affecting a typical design of the high-impedance surface are briefly discussed, leading to the quasiclosed form design approach of Section V.

Fig. 2 shows the measured phase of the reflection coefficient of a typical high-impedance surface approximately 30.4 cm by 40.6 cm in area. The substrate was a low dielectric constant ( $\epsilon_r = 1.07$ ) foam, 30.5-mm thick, while the FSS provided 0.47 pF of capacitance. The periodic unit of the FSS and via array was 10.7 mm. The vias had a radius of 1 mm. The desired operating band for the reflection coefficient was from 0.79 GHz ( $+90^\circ$  point) to 1.52 GHz ( $-90^\circ$  point). The difference between the measured reflection phase and the calculated one is probably due to experimental error given the small size of the AMC tested (barely one wavelength at the low end.) Fig. 3 shows the surface wave suppression bandgap of the same structure measured as the S21 coupling between two radiators communicating with

each other exclusively through the surface waves supported by the structure. The well-known proximity of the surface wave suppression bandedges to the  $+90^\circ$  and  $-90^\circ$  phase points is noted.

## II. EFFECTIVE MEDIUM MODEL

Because of symmetry, the structure is modeled as a two-layer anisotropic uniaxial material in both permittivity and permeability (Fig. 4) with the top layer representing the FSS and the bottom layer representing the via-array substrate. Then, the optical axis lies in the  $z$  direction yielding the following form for the tensor constitutive properties of each layer

$$\bar{\epsilon} = \begin{pmatrix} \epsilon_{xx} & 0 & 0 \\ 0 & \epsilon_{yy} & 0 \\ 0 & 0 & \epsilon_{zz} \end{pmatrix}, \quad \bar{\mu} = \begin{pmatrix} \mu_{xx} & 0 & 0 \\ 0 & \mu_{yy} & 0 \\ 0 & 0 & \mu_{zz} \end{pmatrix}. \quad (1)$$

### A. FSS Layer

The approach to obtain the effective medium model is best explained using the FSS capacitive layer. Consider first the TM case, a wave with its  $E$  field in the  $x$ - $z$  plane and  $H$  field in the  $y$  direction incident on a ‘‘Cohn square’’ FSS in free space (Fig. 5) [6].

By considering the electric field on the plane of the square array it is clear that to first order the electric field nearly vanishes in the space between the edges parallel to the  $x$  direction, thus reducing the square array to a strip array. The well known solution for such an obstacle models it as a shunt admittance in the transmission line of free-space, giving as its input admittance [7]

$$Y_{in} = Y_0 \cdot \left[ 1 + j \cdot \frac{2p}{\pi} \cdot k_{z0} \cdot \ln \left( \csc \frac{\pi g}{2p} \right) \right] \quad (2)$$

where  $Y_0$  is the admittance of free space,  $p$  the periodicity,  $k_{z0}$  the propagation constant of the incident plane wave in the  $z$  direction corresponding to a free space propagation constant

$k_0 = \omega/c$ , and  $g$  the gap between the strips. If however, the FSS layer were modeled as a material layer of thickness “ $t_1$ ” with uniaxial anisotropic properties, the input admittance could also be obtained using the transmission line equation where the Load is the free space behind the FSS and the transmission line is the FSS layer

$$Y_{\text{in}} = Y_0 \frac{\cos k_{z1}t_1 + j \left( \frac{k_{z0}}{\omega \varepsilon_0} \frac{k_{z1}}{k_x} \right) \sin k_{z1}t_1}{\cos k_{z1}t_1 + j \left( \frac{k_{z1}}{\omega \varepsilon_0 \varepsilon_x} \right) \frac{k_{z0}}{k_x} \sin k_{z1}t_1} \quad (3)$$

where  $k_{z1}$  is the  $z$  directed propagation constant in the FSS equivalent material layer, given by

$$\left( \frac{k_{z1}}{k_0} \right)^2 = \mu_y \varepsilon_x - \left( \frac{k_x}{k_0} \right)^2 \frac{\varepsilon_x}{\varepsilon_z} \quad (4)$$

with  $\varepsilon_x$ ,  $\varepsilon_z$  and  $\mu_y$  being the relevant constituent parameters of the material tensor for TM incidence, and  $k_x$  is the propagation constant in the  $x$  direction of the waves in all the layers. Under the assumption that  $t_1$  is small and that the permittivity of the FSS layer in the  $z$  direction and the permeability in the  $y$  direction are 1 (since the ideal FSS is infinitely thin), (3) reduces to

$$Y_{\text{in}} = Y_0 \frac{1 + j \frac{k_{z0}}{k_{z1}} \frac{\omega \varepsilon_0}{\omega \varepsilon_0 \varepsilon_x} k_{z1} t_1}{1 + j \frac{k_{z1}}{k_{z0}} \frac{\omega \varepsilon_0 \varepsilon_x}{k_{z0}} k_{z1} t_1} = Y_0 \frac{1 + j \varepsilon_x k_{z0} t_1}{1 + j \frac{(k_{z1})^2 t_1}{\varepsilon_x k_{z0}}} \quad (5a)$$

and since by (4),  $k_{z1}^2 = k_0^2 \varepsilon_x \left( 1 - (k_x/k_0)^2 \right) = k_0^2 \varepsilon_x (k_{z0}/k_0)^2$  it follows that  $k_{z1}^2/k_{z0} = k_{z0} \varepsilon_x$  and (5a) becomes

$$Y_{\text{in}} = Y_0 \frac{1 + j \varepsilon_x k_{z0} t_1}{1 + j k_{z0} t_1} \approx Y_0 [1 + j \varepsilon_x k_{z0} t_1]. \quad (5b)$$

Comparing (5b) to (2) we conclude that the FSS layer has an effective  $x$  directed relative permittivity equivalent to a pure shunt capacitance that is angle independent given by

$$\varepsilon_x = \frac{2p}{\pi t_1} \cdot \ln \left( \csc \frac{\pi g}{2p} \right). \quad (6)$$

Since the FSS layer is not floating in space but supported by a dielectric substrate, the result of (6) is increased in practice by the average relative permittivity,  $\varepsilon_{\text{avg}}$ , of the dielectric materials surrounding the FSS. This average permittivity is weighted by flux similarly as in quasi-TEM microstrip lines.

The development for TE is identical. The  $z$ -directed propagation constant in the uniaxial medium for TE is given by

$$\left( \frac{k_{z1}}{k_0} \right)^2 = \varepsilon_y \mu_x - \left( \frac{k_x}{k_0} \right)^2 \frac{\mu_x}{\mu_z}. \quad (7)$$

Therefore, the input impedance for the material layer model is given by (8), while the TE incidence result from [7] for the FSS as a shunt obstacle is still given by (2)

$$Y_{\text{in}} = Y_0 \cdot \left[ 1 + j \cdot \frac{k_{z0} t}{\cos^2 \theta} \cdot \left( \varepsilon_y - \sin^2 \theta \cdot \frac{1}{\mu_z} \right) \right]. \quad (8)$$

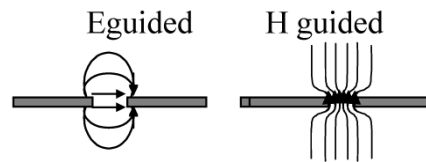


Fig. 6. Strip medium concentrates the E-field lines but it constricts the H-field lines normal to it.

In order for (8) to be equivalent to (2), the  $\theta$ -dependent terms must vanish. This can only happen if

$$\varepsilon_y = \frac{1}{\mu_z} = \frac{2p}{\pi t} \cdot \ln \left( \csc \frac{\pi g}{2p} \right). \quad (9a)$$

This relation shows us that the normal permeability of the strip layer is the inverse of the transverse permittivity because to the extent that the structure concentrates the in-plane E field, to that same degree it squeezes the normal H field (Fig. 6). That this result must be true can be visualized by realizing that this structure (the infinite array of strips) can guide a TEM wave along the length of the strips as if it were a multiconductor transmission line. The electric and magnetic field distributions of that TEM wave are exactly the ones of concern in the derivation of the above effective constitutive properties. The E field is concentrated at the edges of the strips while the H field is squeezed in between the strips. If this infinite array of strips is surrounded by free space on both sides it follows that the TEM wave must travel at the speed of light. Therefore, if the effective permittivity is raised by the concentration of energy at the strips' edges, the effective permeability must be dropped by exactly the same factor, since the product of the two control the speed of propagation along this structure. The depression of the normal permeability is, therefore, a geometric effect proportional to the ratio of gap area to blocking metal area. (Note, that if we were not to consider the normal permeability of the FSS, we would be forced to model the FSS as an angle-dependent shunt capacitance.) Equation (9a) is the result for the strip array FSS. By our original argument of Fig. 5, this result is also approximately correct for the metal square patch array FSS. However, the  $z$ -directed permeability is not as depressed as (9a) suggests because the magnetic field is not as “squeezed.” There are twice as many gaps between conductors per unit cell in a square array as compared to a strip array. Therefore, for an array of Cohn squares

$$\mu_z \cong \frac{2}{\varepsilon_y}. \quad (9b)$$

Again, the presence of the dielectrics supporting the FSS must be taken into account. Since they alter in no way the magnetic field, (9b) is not changed, but the transverse permittivity given by (9a) is increased by  $\varepsilon_{\text{avg}}$ .

### B. Via- Array Region

The lower layer, via-array region, can be regarded as Brown's rodged medium. The solution for this medium can be found in [8] and [9] for thin rods. To account for the possibility of thicker rods, the effective medium model is derived for the unit cell illustrated in Fig. 7 as follows. For E fields aligned with the vias,

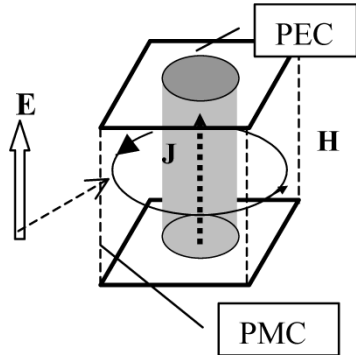


Fig. 7. Unit cell of the via array can be modeled as a single current carrying via capped by PECs and surrounded by PMCs.

the medium can be regarded as highly inductive. This inductance can be calculated from the magnetic energy in the unit cell of side length  $d$  given by  $U_m = 1/2 \int \vec{B} \cdot \vec{H} dv$ . In the low frequency approximation the rod in the unit cell is terminated in PECs of area  $A$  (periodicity  $\sqrt{A} = d$ ) and surrounded by PMCs of height equal to the thickness,  $t_2$ , of the via-array substrate so that the periodic boundary conditions are fulfilled. A closed-form expression is obtained for the magnetic field by using Ampere's law. Setting this result equal to  $U_m = 1/2 I^2 L$ , yields

$$L = \frac{\mu_D \mu_0 \cdot t_2}{4\pi} \left[ \ln \left( \frac{1}{\alpha} \right) + \alpha - 1 \right] \quad (10)$$

where  $\alpha$  is the ratio of the via's cross sectional area to the unit cell area. Here, we define the relative permittivity and permeability of the host dielectric that surrounds the vias as  $\epsilon_D$  and  $\mu_D$ . The effective permittivity of the unit cell in the  $z$  direction is then

$$\epsilon_{zz}(\omega) = \epsilon_D - \frac{1}{\omega^2 \epsilon_0 \frac{\mu_D \mu_0 A}{4\pi} \left[ \ln \left( \frac{1}{\alpha} \right) + \alpha - 1 \right]}. \quad (11)$$

This permittivity is characterized by a negative real part up to a "cutoff" frequency. Above the cutoff frequency it approaches the value of the surrounding medium,  $\epsilon_D$ . It should be noted that the derivation of (11) follows the lines of classic effective medium theory. The inductance of (10) only depends on the areal fraction  $\alpha$  and not on the relative size of the cylinder (or the unit cell) with respect to the wavelength. It can be readily verified that in this low frequency limit of (11), the same effective permittivity can be obtained by a variety of combinations of the absolute size of the unit cell (given by  $\sqrt{A}$ ) and the areal fraction. As will be shown below, the fact that the effective permittivity of (11) is negative controls the types of TM surface waves that can propagate on this structure. It further turns out that when this negative value is of the order of  $-100$  to  $-10$ , there appears a band of frequencies over which those surface waves cannot propagate. Thus the surface wave cutoff or beginning of the stopband for TM surface waves is controlled by the average value of the normal permittivity and not by the onset of Bragg scattering as is common with the traditional EBG structures. Having said this, we desire the most accurate possible model of this permittivity and, therefore, we should include the breakdown of the effective medium model as the wavelength

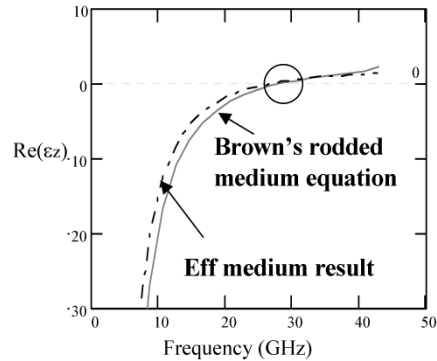


Fig. 8. Permittivity in the  $z$  direction of the effective medium model agrees with Brown's solution.

approaches the size of the unit cell. This is accomplished by invoking Brown's solution to the rodded medium.

Brown's solution is given as the frequency-dependent index of refraction of the medium, in (12)

$$n = a \cos \left( \cos \left( \frac{2\pi d}{\lambda} \right) + \frac{\lambda}{2d} \left( \frac{\sin \left( \frac{2\pi d}{\lambda} \right)}{\ln \left( \frac{d}{2\pi a} \right) + F \left( \frac{d}{\lambda} \right)} \right) \right) \cdot \frac{\lambda_0}{2\pi d} \quad (12)$$

where  $d$  is the unit cell size,  $F(d/\lambda)$  is a correction factor and  $a$  is the radius of the rods. Fig. 8 shows the real part of the effective permittivity as calculated from (11) and (12) for the rodded medium parameters. Evaluation of (12) near the Bragg scatter limit shows that the effective permittivity rapidly becomes positive and greater than 1. Clearly, at that point the medium ceases to behave as a bed of nails and actually behaves as a grounded dielectric slab, capable of supporting TM surface waves again. Therefore, we reach the conclusion that for this medium, the Bragg-scatter effects actually truncate the bandgap rather than initiate it.

The transverse permittivity of the rodded medium is simply the 2-D Clausius-Mossotti expression

$$\epsilon_{xx} = \epsilon_{yy} = \epsilon_D \left( \frac{1 + \alpha}{1 - \alpha} \right). \quad (13)$$

The transverse permeability is obtained from an argument similar to that used in explaining (9). Assuming a TEM wave traveling along the vias at the speed of light the effective increase of the  $x$  directed ( $y$  directed) permittivity above its dielectric background must be exactly offset by a decrease of the  $y$  directed ( $x$  directed) permeability. Therefore

$$\mu_{xx} = \mu_{yy} = \left( \frac{\epsilon_D}{\epsilon_{xx}} \right) \cdot \mu_D. \quad (14)$$

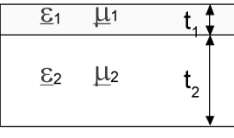
In this way, all the components of the tensors shown in (1) have been determined from effective medium considerations. Table I summarizes the results.

### III. DETERMINING THE REFLECTION AND SURFACE WAVE PROPERTIES

#### A. Reflection Coefficient

The interaction of an incident free space wave with the high-impedance surface can be modeled as a transmission line

TABLE I  
SUMMARY OF THE EFFECTIVE MEDIUM ANISOTROPIC PROPERTIES OF THE 2-LAYER MODEL OF THE SIEVENPIPER HIGH-IMPEDANCE SURFACE

|   |   |
|---|---|
|  | $\underline{\underline{\epsilon}} = \begin{pmatrix} \epsilon_{tran} & 0 & 0 \\ 0 & \epsilon_{tran} & 0 \\ 0 & 0 & \epsilon_{zz} \end{pmatrix} \quad \underline{\underline{\mu}} = \begin{pmatrix} \mu_{tran} & 0 & 0 \\ 0 & \mu_{tran} & 0 \\ 0 & 0 & \mu_{zz} \end{pmatrix}$ |
|---|---|

---

|   |  |
|---|--|
| $\epsilon_{1tran} = \frac{2b}{\pi t_1} \ln\left(\frac{2b}{\pi g}\right) \epsilon_{avg}$ $\epsilon_{1zz} = 1$ $\mu_{1tran} = \mu_D$ $\mu_{1zz} = \frac{2\epsilon_{avg}}{\epsilon_{1yy}} \mu_D$ | $\epsilon_{2tran} = \epsilon_D \left(\frac{1+\alpha}{1-\alpha}\right)$ $\epsilon_{2zz} = \epsilon_D - \frac{1}{\omega^2 \epsilon_0 \frac{\mu A}{4\pi} \left[\ln\left(\frac{1}{\alpha}\right) + \alpha - 1\right]}$ $\mu_{2tran} = \frac{\epsilon_D}{\epsilon_{2tran}} \mu_D \quad \mu_{2zz} = (1-\alpha)\mu_D$ |
|---|--|

problem. The equivalent circuit is that of a shorted section of transmission line of length  $t_2$  with a shunt capacitance in front of it representing the FSS. With the assumption of a thin structure, the shorted length of transmission line can be replaced by its total series inductance,  $L = \mu_r \mu_0 t_2$  which is then in series with the FSS capacitor to form a series LC circuit, resonant at the frequency  $\omega_0 = (LC)^{-1/2}$ . Therefore, the reflection coefficient can be expressed as a function of frequency as given in (15).

$$\Gamma = \frac{j\omega t_2 \mu_r \mu_0 - \eta_0 \left(1 - \left(\frac{\omega}{\omega_0}\right)^2\right)}{j\omega t_2 \mu_r \mu_0 + \eta_0 \left(1 - \left(\frac{\omega}{\omega_0}\right)^2\right)} \quad (15)$$

where  $\eta_0$  is the impedance of free space,  $\mu_r \mu_0$  is the transverse permeability of the substrate and  $\omega$  the frequency in rad/s. Traditionally, the frequency range over which the reflection coefficient phase switches from  $+90^\circ$  to  $-90^\circ$  is considered the operating band of the high-impedance surface, since over this band the image of a horizontal current source always adds gain to its radiation pattern. Then, calling  $f_{upper}$  the frequency at which the phase of the reflection coefficient crosses  $-90^\circ$ , and  $f_{lower}$  the frequency at which it crosses  $+90^\circ$  it is easy to show that for thin high-impedance surfaces, the bandwidth,  $BW = f_{upper}/f_{lower}$ , is given by

$$\frac{BW - 1}{\sqrt{BW}} = 2\pi \mu_r \frac{t_2}{\lambda_0}. \quad (16)$$

Fig. 9 shows the Reflection coefficient phase as a function of frequency for a high impedance surface 0.062-in thick, with a 4.5 dielectric substrate and an FSS supplying a shunt capacitance of 0.4 pF, tuned to a center frequency of 5.5 GHz and a bandwidth of 1.2.

### B. Surface Wave Properties

Following [9], the via-array is treated as a ‘‘Fakir’s bed of nails’’ wave-guiding surface. To find the propagation constant we apply the transverse resonance method (TRM), with its convenient transmission line analogy. Assuming surface wave

propagation in the  $x$  direction all layers of the multilayer medium—air/FSS/via substrate/ground plane—share the same  $k_x$ . In addition to the  $z$  direction propagation constants given in (4) (TM) and (7) (TE) we need the corresponding medium impedances. These are given in (17)

$$Z_{TM} = \frac{k_z}{\omega \epsilon_x \epsilon_0}, \quad Z_{TE} = \frac{\omega \mu_0 \mu_x}{k_z}. \quad (17)$$

From this point on subscript 2 refers to the lowest layer, that is the via-array substrate, and subscript 1 refers to the upper FSS layer. Applying the TRM at the boundary between air and the FSS layer we find the properties of TM and TE waves.

### C. TM Waves

The impedance looking to the right is the short circuit of the ground-plane rolled through the two sections of the two-layer material transmission line

$$Z_{in} = \frac{k_{z1}}{\omega \epsilon_0 \epsilon_{x1}} \cdot \frac{j \frac{k_{z2}}{\omega \epsilon_0 \epsilon_{x2}} \tan(k_{z2} t_2) \cos(k_{z1} t_1) + j \frac{k_{z1}}{\omega \epsilon_0 \epsilon_{x1}} \sin(k_{z1} t_1)}{\frac{k_{z1}}{\omega \epsilon_0 \epsilon_{x1}} \cos(k_{z1} t_1) - \frac{k_{z2}}{\omega \epsilon_0 \epsilon_{x2}} \tan(k_{z2} t_2) \sin(k_{z1} t_1)}. \quad (18)$$

The impedance looking to the left is that of a surface wave in free space with  $z$  decay constant  $\alpha$

$$Z_{left} = \frac{k_{z0}}{\omega \epsilon_0} = \frac{\alpha}{j\omega \epsilon_0}. \quad (19)$$

Setting the impedance looking to the left equal to the negative of the impedance looking to the right, yields

$$\alpha = \frac{k_{z1} \frac{k_{z2}}{k_0 \epsilon_{x2}} \tan(k_{z2} t_2) \cos(k_{z1} t_1) + \frac{k_{z1}}{k_0 \epsilon_{x1}} \sin(k_{z1} t_1)}{\epsilon_{x1} \frac{k_{z1}}{k_0 \epsilon_{x1}} \cos(k_{z1} t_1) - \frac{k_{z2}}{k_0 \epsilon_{x2}} \tan(k_{z2} t_2) \sin(k_{z1} t_1)}. \quad (20a)$$

But since  $kx = \sqrt{k_0^2 + \alpha^2}$  we obtain an equation of the form

$$k_x (TM) = \sqrt{k_0^2 + \alpha (k_{z1}(k_x), k_{z2}(k_x))^2}. \quad (20b)$$

A graphical solution of (20) is most instructive. For a lossless structure guiding slow waves, we input real valued  $k_x > k_0$ ,

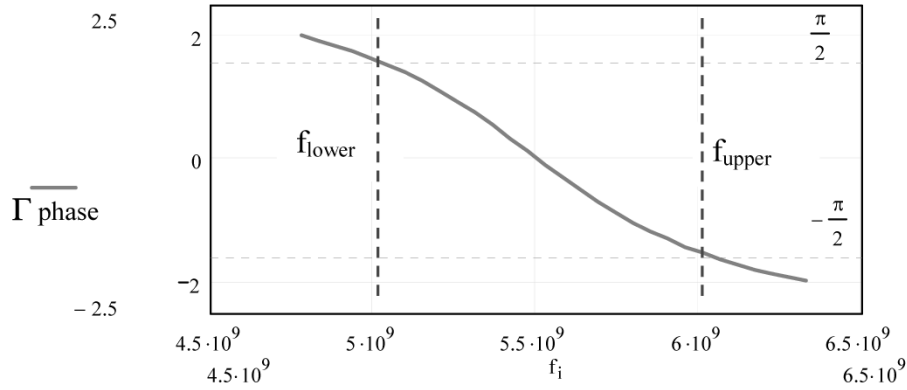


Fig. 9. Typical reflection coefficient phase for a Sievenpiper-like high-impedance surface.

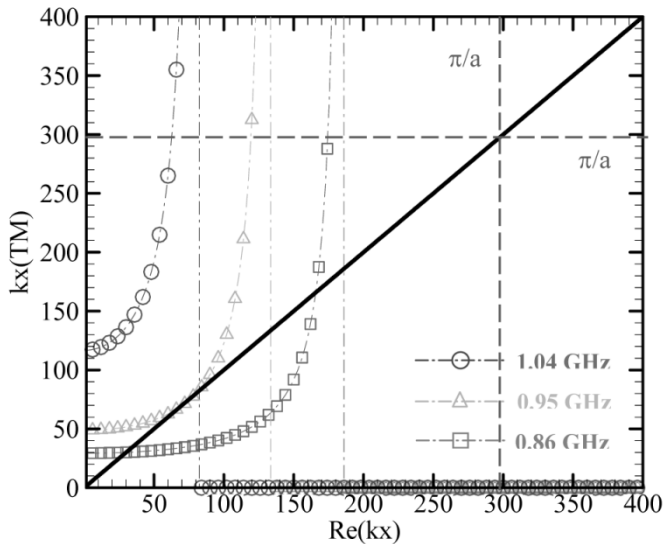


Fig. 10. Graphical solution of the TM guided waves.

into the right hand side of (20b) and where the equation  $y = k_x(TM)$  intersects the line  $y = k_x$ , we have a propagating guided wave. Fig. 10 shows a typical solution for a structure like that of Figs. 2 and 3 but with vias spaced much more closely (period = 5.4 mm, via diameter = 0.5 mm,  $t_2 = 32$  mm,  $\epsilon_D = 1.07$ ). It has the same characteristics as King and Park's Fakir structure. As those authors mention, in addition to the first two solutions there are an infinite number of additional intersections, with an infinite number of tangent-like curves (higher order modes). However those intersections correspond to modes of extremely high reactance, which would exist only extremely close to the surface. Furthermore, they correspond in the example to values of  $k_x$  that exceed the periodic unit limit  $\pi/d$ , therefore, they are not relevant to the physical situation. As the figure shows, as frequency is increased, the two lowest order modes approach each other and coalesce, and then exit the lower order mode curve. At this point, if no higher order mode curves exist within the periodic unit limit, there are suddenly no allowed TM modes. This is the TM cutoff, or lower surface-wave suppression band edge of the Sievenpiper structure. It is caused by the effect the negative  $\epsilon_{zz}$  of the via-array substrate has on the  $z$  directed propagation constant [see (4)]. When this calculation is carried out for the structure of Figs. 2 and 3, the predicted

TM surface wave cutoff is 952 MHz. This is within 3% of the measured result of 981 MHz.

In the case of Fig. 10, the surface-wave suppression starts near 1 GHz. This frequency may be changed by simply changing the value of the negative permittivity, that is, by changing the parameters of the via-array. As a rule the lowest frequency band edge (and, therefore, the broadest bandgap) is obtained by operating in a regime where the negative axial permittivity is in the range between  $-50$  and  $0$ . This can be obtained, for example, by either increasing the periodic unit or decreasing the radius of the vias. Changing the periodic unit has a stronger effect in the value of the inductance than changing the radius of the vias. Thus the strongest control parameter for the position of the lower surface-wave suppression band edge is the periodic unit of the via-array. However, there is a limit to how far we can go with this control parameter because increasing the via separation moves the operating band closer and closer to the Bragg-scatter limit and, as has been pointed out above, we run the risk of losing the negative value of the axial permittivity. Nevertheless, it is clear that this band edge may or may not fall near the frequency at which the phase of the reflection coefficient of the surface crosses  $+90^\circ$ .

#### D. TE Waves

Following the same procedure as in the TM waves, but using the wave admittance, leads us to the corresponding equations. The admittance looking to the right is the admittance of the short circuit rolled through the two layers and the admittance looking to the left is that of a surface wave in free space with  $z$ -decay constant  $\alpha$

$$Y_{\text{in}} = \frac{k_{z1}}{\omega\mu_0\mu_{x1}} \cdot \frac{-j\frac{k_{z2}}{\omega\mu_0\mu_{x2}} \cot(k_{z2}t_2) \cos(k_{z1}t_1) + j\frac{k_{z1}}{\omega\mu_0\mu_{x1}} \sin(k_{z1}t_1)}{\frac{k_{z1}}{\omega\mu_0\mu_{x1}} \cos(k_{z1}t_1) + \frac{k_{z2}}{\omega\mu_0\mu_{x2}} \cot(k_{z2}t_2) \sin(k_{z1}t_1)} \quad (21a)$$

$$Y_{\text{left}} = \frac{k_{z0}}{\omega\mu_0} = \frac{-j\alpha}{\omega\mu_0} \quad (21b)$$

Again solving for  $\alpha$ , and setting  $k_x = \sqrt{k_0^2 + \alpha^2}$  yields an equation of the form

$$k_x(TE) = \sqrt{k_0^2 + \alpha(k_{z1}(k_x), k_{z2}(k_x))^2} \quad (22)$$

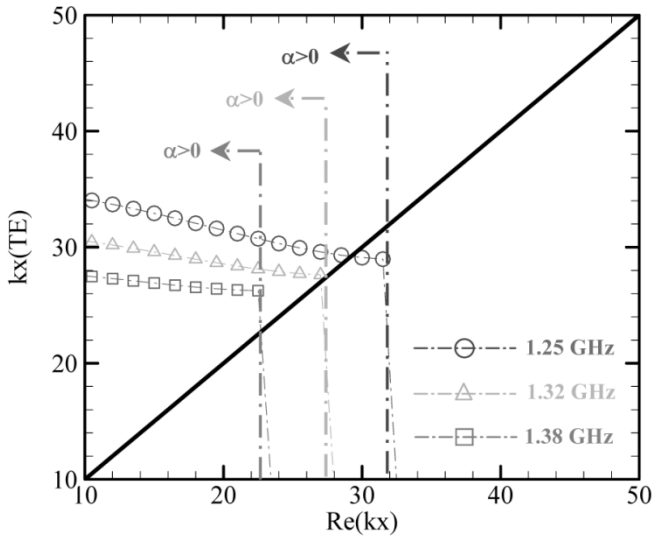


Fig. 11. Graphical solution of the TE guided waves. Proper solutions only exist when the intersection occurs at  $\alpha > 0$ .

We will use, again, a graphical solution for this problem. Only when the intersection occurs for  $\alpha > 0$  do we have a physically realizable guided wave. Intersections at  $\alpha < 0$  are improper (nonphysical) modes that do not exist. The graphical solution is illustrated in Fig. 11. Overlaid over the solution are the boundaries where  $\alpha$  changes from positive to negative. At those boundaries the solid curve representing the right hand side of (22) is stopped, because after that point the solution is a non-physical mode. When this procedure is carried out for the High Impedance Surface of Figs. 2 and 3, the TE band edge is calculated to be at 1.32 GHz, which is within 3% of the measured band edge.

As the frequency is raised above the frequency at which the phase of the reflection coefficient of the surface crosses zero degrees, the right-hand side of (22) approaches the  $y = k_x$  line. Onset of TE guided waves occurs at the point of intersection. This is the TE or upper surface-wave suppression band edge of the high-impedance surface. It is caused by the effect the depressed  $\mu_{zz}$  of the FSS layer has on the  $z$ -directed propagation constant [see (7)]. Therefore, the position of this band edge can be changed by dropping  $\mu_{zz}$ , for instance by changing the geometrical shape of the FSS layer. When  $\mu_{zz}$  is dropped by a factor of two the intersection moves from 1.32 GHz to 1.46 GHz (Fig. 12).

In summary, the surface-wave suppression bandwidth of the Sievenpiper high-impedance surface is controlled by the negative value of the normal permittivity of the via-array substrate and the depressed normal permeability of the FSS layer. The position of the band edges relative to the  $+90^\circ$  or  $-90^\circ$  phase shift points of the reflection coefficient is in general arbitrary except for the fact that the TE band edge can only occur above the zero degree phase frequency (the reflection coefficient resonance). Because of the zero degree phase reflection coefficient at the center of its operating band, we refer to these high-impedance surfaces as artificial magnetic conductors (AMCs). The physical implementation of these structures is treated in the next section.

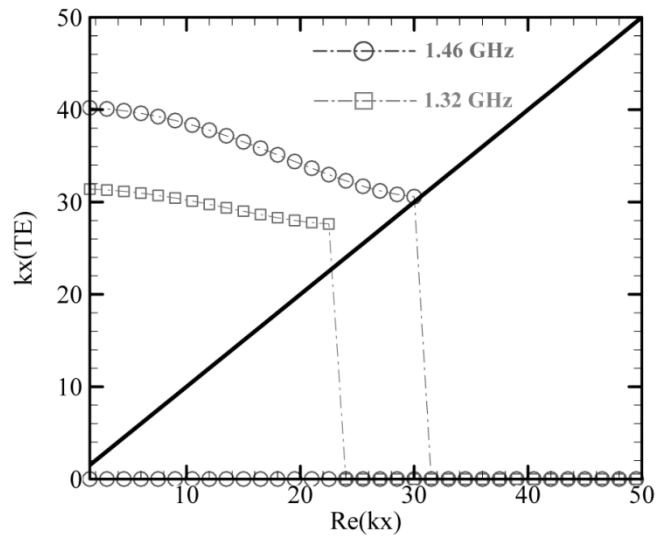


Fig. 12. TE band edge increased after halving  $\mu_z$ .

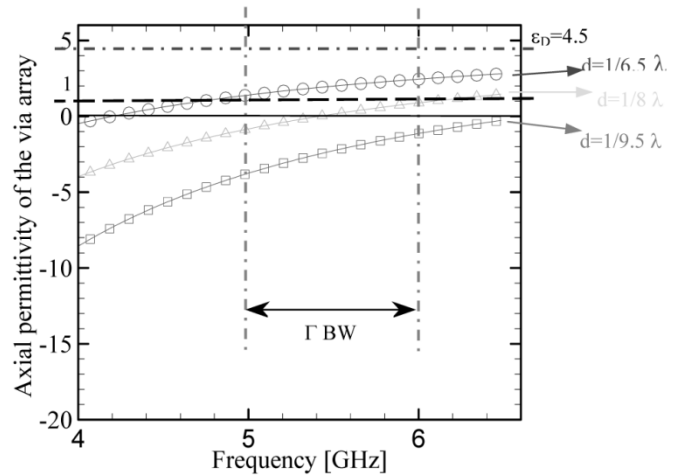


Fig. 13. Real part of the axial permittivity of the substrate as a function of frequency for a substrate of  $\epsilon_r = 4.5$  and different via spacings. The  $+90^\circ$  and  $-90^\circ$  reflection coefficient bandwidth ( $\Gamma$  BW) is shown for reference.

#### IV. PHYSICAL REALIZATION OF THE SIEVENPIPER FAMILY OF AMCS

##### A. BW of TM Surface Waves

The via-array is the region of the AMC that governs the behavior of TM surface waves. TM cutoff occurs, as mentioned before, when the value of  $\epsilon_{zz}$  is negative. In Fig. 8 we saw that this permittivity is a strong function of frequency, hence, the importance of choosing the right value of inductance for the via array region in regards to the bandwidth. Clearly, if the value of the normal permittivity of the substrate becomes greater than one it will be able to support conventional surface waves. Thus the most general guideline to insure surface wave suppression is to maintain the normal permittivity less than one within the bandwidth of interest. Additionally, for a Fakir's bed of nails type of cutoff to occur, the normal permittivity must be negative at the lower band edge.

Given a choice of substrate dielectric constant, the normal permittivity is controlled over the band by controlling the zero-crossing frequency, that is when  $\epsilon_{zz} = 0$ . Fig. 13 illustrates the



effect of the via spacing on this crossing for a substrate whose relative dielectric constant is 4.5. The vertical lines define the extent of the  $+/-90^\circ$  reflection phase bandwidth. In this Figure the case when the vias are  $1/9.5$  of a free space wavelength apart (at the reflection phase resonance) gives the most negative normal permittivity because its zero-crossing frequency is far above the high-impedance frequency band of operation. However it also gives the most rapidly varying value of  $\epsilon_{zz}$  over the band, and this turns out to limit the surface wave suppression bandwidth. To maximize the bandwidth we want the slowest possible varying normal permittivity that nevertheless does not cross 1 inside the band of operation. Therefore, for this case a via spacing of the order of  $1/8$  of a wavelength would be the best choice. Clearly, in Fig. 13 the dielectric constant of the substrate plays an important role in the determination of the bandwidth because it controls the asymptotic high frequency limit of  $\epsilon_{zz}$ , and, therefore, the slope of the curve over the bandwidth of operation. If the permittivity of the substrate is too high, then the zero crossing value will appear lower in frequency, diminishing – in this way — the possible available surface wave suppression bandwidth. This tradeoff exercise will become clear in the following section when we find closed form versions of the transverse resonance solution. As a rule of thumb it is advisable to put the zero crossing as close as possible to the upper end of the band.

### B. BW of TE Surface Waves

As seen, TE surface waves do not occur until a certain onset frequency, or cutoff frequency. This means that the TE case has an intrinsic surface wave suppression band that starts at zero frequency. In this respect the AMC is similar to a grounded dielectric slab that in general exhibits this onset point near the frequency at which the reflection phase crosses zero degrees. The effect of the depressed  $\mu_{zz}$  of the FSS is to push this onset frequency above that point. The lower the normal permeability, the higher this onset of TE waves is pushed. In other words, the effectiveness of the FSS in blocking the normal magnetic field determines the TE mode cutoff frequency, and hence the TE bandwidth.

When a normal magnetic field cuts into a metal obstacle, eddy currents are formed, which oppose the incident field and force it to flow through gaps in the structure. The blockage is, therefore, mainly a function of the geometric shape of the FSS. In our example of a square shaped FSS patch, the blockage is approximately half that of a strip array floating in free space. This means that the value of the normal permeability is approximately  $2/\epsilon_{yy}$ . Full-wave modeling of the unit cell readily proves this. Since the metal squares are supported by a dielectric substrate, their capacitance and, therefore, their transverse permittivity is increased without adding blockage. Therefore, the normal permeability's value for a dielectric-supported array of metal squares is

$$\mu_{zz} = \frac{2}{\epsilon_{\text{geom}}}, \quad \epsilon_{\text{geom}} = \frac{\epsilon_{xx}}{\epsilon_{\text{average}}}. \quad (23)$$

Where  $\epsilon_{\text{average}}$  is the average permittivity of the medium that surrounds the metal squares (as explained earlier in the paper).

In summary, if we want to suppress TE surface waves we have to allow for the normal H field to be blocked as much as needed in order to meet the TE band requirement. FSS consisting of metal squares are maximally blocking while FSS consisting of crossed dipoles would be minimally blocking. Finally, the blocking performance of the FSS is indirectly affected by the thickness and composition of the via-array substrate because to obtain zero degree phase in the reflection coefficient at the desired center frequency the total phase shift supplied by the FSS and the substrate must be equivalent to one quarter wavelength. Therefore, if the substrate is made too thick, or has too high a dielectric constant, the FSS capacitance will be too small, and hence the FSS patches will be too small or the gaps will be too large to adequately block the normal magnetic field.

Different kinds of antennas may or may not need both surface-wave suppression bands. For example, horizontal antennas radiate mainly TE waves. The Sievenpiper family of AMCs can be designed to have a  $+/-90^\circ$  reflection coefficient phase operating band coincident with either TE only, TM only, or both surface wave band gaps. The two extremes are as follows.

- TM-only suppression band—In this case, the suppression of TM surface waves is of interest and the suppression of TE surface waves is assumed to be irrelevant. The FSS layer needs to provide the additional phase difference using its capacitance but is not required to obstruct the normal magnetic field, thus allowing the TE surface waves to propagate in the medium. A Jerusalem-cross shaped element is, therefore, assumed for the FSS.
- TE-only suppression band—In this case, TM surface waves are not a concern, therefore, we can position the zero crossing value of  $\epsilon_{zz}$  of the via array well inside the band. In fact we do not even need the via-array to suppress only TE surface waves.

But to answer the general question of how to get a certain bandwidth for the reflection coefficient, and TE and TM suppression independently or arbitrarily, we need a design methodology, i.e., a closed form solution.

## V. QUASI-CLOSEDFORM SOLUTIONS

The graphical solutions give us great insight on the behavior of the structure however a closed form solution with frequency as its independent variable would allow us much more flexibility for the design of these types of AMCs. In this section we will derive quasiclosed form solutions for this purpose, based on certain reasonable approximations.

### A. TM Case

For the TM modeling we can assume that the structure is a grounded slab with a shunt capacitance  $C$  in parallel to it as shown by the discussion leading to (6). Applying the TRM to this transmission line analogy and taking advantage of the fact that the slab is by definition electrically thin—therefore, the tangent functions approximate to their arguments; we arrive at the following expression that is a simplified version of (20)

$$kx_{\text{TM}} = \sqrt{\frac{\epsilon_0^2 (kz_2)^2}{(C \cdot kz_2 - \epsilon_0 \epsilon_{xx2} \cot(kz_2 \cdot t_2))^2} + k_0^2}. \quad (24)$$

Where  $k_{z2}$  is the  $z$ -directed propagation constant inside the anisotropic via-array substrate.

By noting in Fig. 10 the resemblance between the curves from the right hand side of (20b) to secant functions we realize that there are only two parameters to be determined: (1) the value of  $k_x$  when the function goes to infinity and (2) the value of the function when  $k_{xTM}$  is equal to zero.

We will first find the value of the function for  $k_x = 0$

$$k_{xTM}|_{k_x=0} = k_0 \sqrt{\frac{\varepsilon_0^2 \varepsilon_{xx2} \mu_{yy2}}{(C \cdot k_0 \sqrt{\varepsilon_{xx2} \mu_{yy2}} - \varepsilon_0 \varepsilon_{xx2} \cot(k_0 \sqrt{\varepsilon_{xx2} \mu_{yy2}} \cdot t_2))^2 + 1}} \quad (25)$$

Now to identify where the infinity point is we just have to find the value of  $k_x$  so that the denominator of (24) is equal to zero. Then, the infinity point is

$$k_{xTM\infty} = k_0 \sqrt{\mu_{yy2} \varepsilon_{zz2} \left( 1 - \left( \frac{k_{res}}{k_0} \right)^2 \right)} \quad (26)$$

where  $k_{res} = k_0$  at the resonant frequency. Now, we will just use the following secant function to represent the lowest order mode curve of the TM case.

$$y = (k_{xTM}|_{k_x=0}) \cdot \sec\left(\frac{\pi}{2 \cdot k_{xTM\infty}} k_x\right). \quad (27)$$

In the previous section, it was shown (Fig. 10) that the curves move from right to left when the frequency is increased. So the band edge will happen when the lowest order mode curve of Fig. 10 leaves the  $45^\circ$   $k_x$  line. In this way we identify the TM band edge. To find this point using (24) we first find the point at which the derivative of (27) is one (the slope of the curve  $y = k_x$ ). After working out the derivative of (27) we encounter as an intermediate step a quadratic equation in sine functions. The solution of that quadratic equation is

$$U = \frac{-\pi (k_{xTM}|_{k_x=0})}{4 \cdot k_{xTM\infty}} + \sqrt{\left(\frac{\pi \cdot k_{xTM}|_{k_x=0}}{4 \cdot k_{xTM\infty}}\right)^2 + 1}. \quad (28a)$$

The point of interest turns out to be the arcsine function of (28a) multiplied by a constant ,

$$KX_{TM} = \frac{2 \cdot k_{xTM\infty}}{\pi} a \sin(U). \quad (28b)$$

Substituting  $KX_{TM}$  from (28b) for the  $k_x$  of (27) we find the ordinate of this point. When this ordinate equals  $KX_{TM}$  itself we have the desired intersection with the  $y = k_x$  line. Thus, if we plot

$$y_{TM} = (k_{xTM}|_{k_x=0}) \cdot \sec\left(\frac{\pi}{2 \cdot k_{xTM\infty}} KX_{TM}\right) - KX_{TM} \quad (28c)$$

as a function of  $k_0$ , the cutoff frequency occurs at the  $k_0$  when  $y_{TM} = 0$ . Fig. 14 shows this exercise for the case of an AMC with center frequency at 5.5 GHz for various via spacings. The frequency of the TM band edge is clearly identified. From Fig. 14 we see that the maximum bandwidth is attained with vias spaced as far apart as possible.

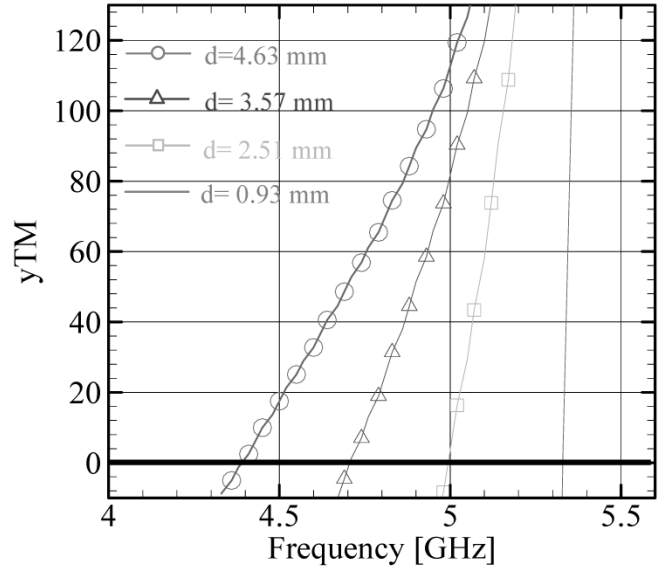


Fig. 14. Plot of the closed form solution for the TM surface wave suppression band edge, (28c).

### B. TE Case

Using similar approximations with respect to the thickness of the via array layer, and also noticing that the FSS layer has a fictitious thickness, we can approximate (22) by

$$k_{xTE} = k_0 \sqrt{\frac{\left[ \mu_{xx1} - \mu_{xx2} c_2 t_1 (k_0)^2 \left( \mu_{xx1} \varepsilon_{yy1} - \left( \frac{k_{xTE}}{k_0} \right)^2 \frac{\mu_{xx1}}{\mu_{zz1}} \right) \right]^2}{(\mu_{xx1} k_0)^2 (\mu_{xx2} c_2 + \mu_{xx1} t_1)^2} + 1} \quad (29)$$

where:  $c_2 = \tan(k_0 \sqrt{\varepsilon_{y2} - 1} \cdot t_2) / k_0 \sqrt{\varepsilon_{y2} - 1}$  is simply a proportionality constant. Equation (29) is a second order polynomial in  $k_{xTE}$  squared. Therefore it yields four closed form values for  $k_{xTE}$ . Only real values correspond to guided waves; and only those real values occurring with  $\alpha > 0$  are physically possible. Setting  $\alpha = 0$  in the transverse resonance equations yields.

$$k_x|_{\alpha=0} = \sqrt{\left( k_0^2 \varepsilon_{yy1} - \frac{1}{\mu_{xx2} c_2 t_1} \right) \mu_{zz1}}. \quad (30)$$

Therefore, only the real roots of (29) with  $k_x$  less than the value of (30) are physically realizable guided surface waves.

Equation (29) for the quasiclosed form solutions of the TE case is plotted in Fig. 15 only as an aid to visualize the concept. The analytically derived intersections with the  $y = k_x$  line (real roots) are the highlighted points in the figure. In the figure we plotted (29) and the boundary at which  $\alpha$  crosses zero for the resonance frequency ( $f_1$ ) and for a 1.11 times that frequency ( $f_2$ ). Clearly the TE surface waves are suppressed at the resonance frequency since the boundary at which  $\alpha_1 = 0$  occurs at  $k_x = 0$  and no real solutions exist for (29). On the other hand, as the frequency increases, the  $\alpha_2 > 0$  region increases and the complex solutions of (29) begin to coalesce to the real axis of the complex plane. The real solution shown in Fig. 15 for frequency  $f_2$  happens in two points, one outside the  $\alpha_2 > 0$  region

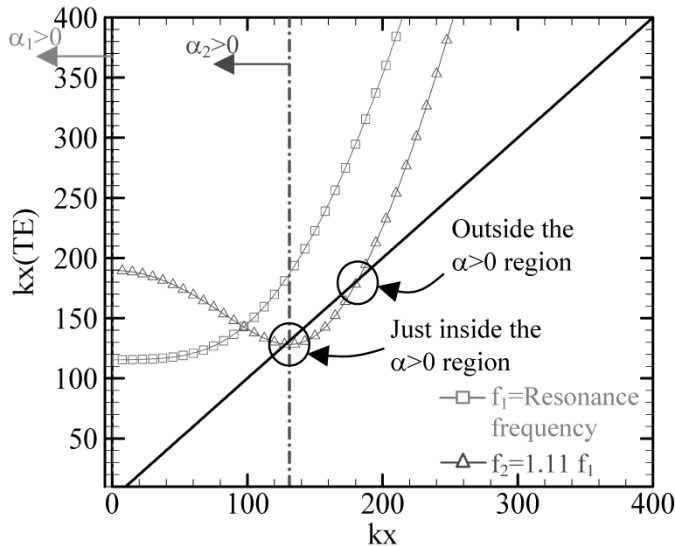


Fig. 15. Plot of (29),  $k_x \text{TE}(k_x)$ , and the equation  $y = kx$  to show the intersection points derived in closed form from (29) and (30). Two frequencies are shown,  $f_1 = 5.5$  GHz (resonance or band center of  $\Gamma$ ) and  $f_2 = 6.1$  GHz. The boundary where  $\alpha$  crosses zero is superimposed for each frequency to illustrate how (30) selects the correct solution. In this case TE onset occurs at 6.1 GHz.

(nonphysical solution) and the other exactly inside the region. Hence, a TE surface wave is excited for frequency 1.11 times the resonance frequency and this is the TE bandedge.

Solutions from the quasiclosed form equations just derived can be compared to an AMC modeled using a finite-element calculation [10]. The AMC modeled was a 1.6-mm thick with substrate dielectric constant of 2.2, periodicity of 2.4 mm, rod radius of 0.36 mm, and a square FSS capacitance of 0.07 pF (equivalent to 12 GHz center frequency). Fig. 10 in [10] shows a surface wave bandgap from 10 to almost 15 GHz. Using our quasiclosed form model the bandgap spans from 9.8 to 14.7 GHz.

Using these quasiclosed form equations we can appreciate the full range of options available to the designer. In Fig. 16, the TE quasiclosed form solution is used to determine the effect that dropping the normal permeability of the FSS layer has on the bandwidth. We plot as ordinate the relative propagation constant of the guided waves ( $k_x/k_0$ ), so that whenever this ratio is greater than 1.0 we have guided slow waves. First the solution of an AMC without magnetic field blockage is found. In this case slow TE surface waves would be excited very close to the resonance frequency, within the band of interest (5 to 6 GHz). This is illustrated with the blue line in Fig. 16. However, assuming an FSS with metal squares to block the normal H field, our band of surface wave suppression is expanded even beyond the desired band edge (the  $-90^\circ$  point of the reflection coefficient).

A method for the design of this type of AMCs may take the following form. The center frequency will be the first data needed for the design. Then, either bandwidth or structure's thickness can be assumed as the input parameters. One would lead to the other one by simply enforcing the behavior of the structure's reflection coefficient response within the desired bandwidth according to (16). Once the pertinent permittivities of the substrates are input and using our closed-form solutions, the adequate periodicity and rod radius can be found so that surface waves do not propagate within our band of interest.

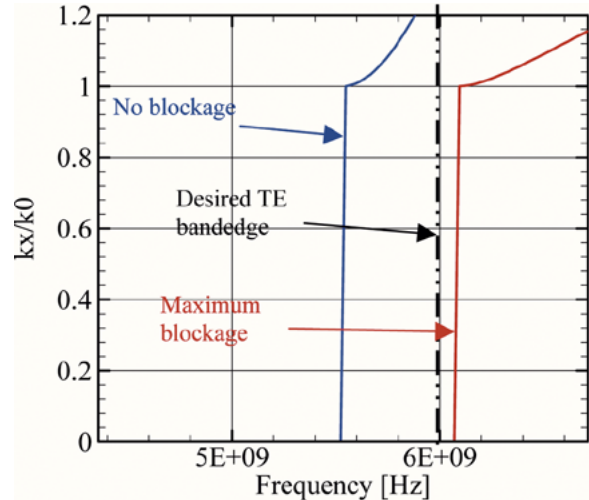


Fig. 16. Plot of the relative propagation constant of the guided TE surface waves versus frequency showing the onset of guided waves for the case of  $\mu_z = 1$  (no H-field blockage by FSS) and the case of an FSS using metal square patches (maximum blockage).

Finally, assuming square elements in the FSS layer, the TE surface waves can be suppressed within the band of interest using the closed-form models.

Thus it has been shown that we can independently design the upper and lower surface wave suppression bandedges by simply changing certain parameters of the AMC. In the following section the design space is narrowed to two parameters, thickness and dielectric constant of the substrate, for a maximum bandwidth design.

### C. Maximum Bandwidth Design

Naturally, having a broad bandwidth of operation is one of the most important requirements. After all this discussion it is clear that the thickness and the permittivity of the substrate directly or indirectly affect both TE and TM surface wave suppression bandwidths. Therefore we make these parameters variables and calculate the available TM, TE, and total bandwidth based on the quasiclosed form expressions. A design with resonant frequency at 5.5 GHz is assumed. The results are the contour plots of Fig. 17 showing the maximum fractional bandwidths ( $f_{\text{upper}} - f_{\text{lower}}/f_{\text{res}}$ ) possible as a function of substrate thickness and permittivity. In the  $x$  axis we have different values for the AMCs thickness ranging from  $\lambda/20$  to  $\lambda/4$  and in the  $y$  axis the values of the substrate permittivity ranging from 1.2 to 10.

For the TM case, as the substrate thickness and dielectric constant are changed, the via spacing is automatically adjusted to keep the frequency at which  $\epsilon_{zz}$  of the substrate crosses zero at the resonant frequency of the AMC. Then the fractional bandwidth for TM is defined as  $(f_{\text{res}} - f_{\text{TM}})/f_{\text{res}}$ . For the TE case the fractional bandwidth is defined as  $(f_{\text{TE}} - f_{\text{res}})/f_{\text{res}}$ . We can appreciate the tradeoff between thickness and dielectric constant. The upper right corner of the plots is a forbidden region where the combination of dielectric constant and thickness would make the structure's electrical thickness greater than  $\lambda/4$ . We note that the TM bandwidth is strongly limited by the dielectric constant of the substrate. The TE bandwidth, on the other hand, is much more forgiving. Fig. 18 shows the total surface wave suppression bandwidth (given by  $(f_{\text{TE}} - f_{\text{TM}})/f_{\text{res}}$ )

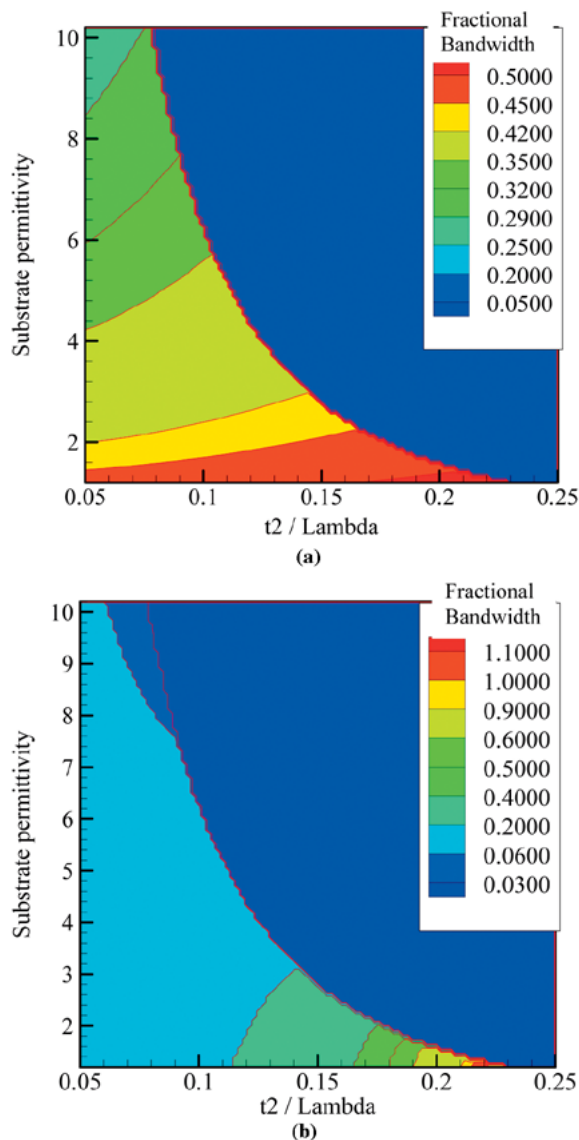


Fig. 17. (a) Contours of available TM fractional bandwidth as a function of substrate thickness and permittivity for a design resonant at 5.5 GHz. (b) Contours of available TE fractional bandwidth as a function of substrate thickness and permittivity for a design resonant at 5.5 GHz.

available to the designer. Note, that if a total bandwidth of operation is all that is desired it can be achieved through various mixes of TE and TM bandwidths.

## VI. CONCLUSION

A two-layer anisotropic uniaxial effective medium model for the Sievenpiper-like high-impedance surface has been developed and used to study the surface-wave suppression properties of this artificial magnetic conductor. The parameters governing the surface wave suppression have been shown to be the normal components of the permittivity and permeability tensor. After simplifying the equations it is possible to obtain contour plots in the design space of substrate thickness versus dielectric constant that portray the maximum possible bandwidth attainable with a given AMC. Once the desired bandwidth is found, the effective medium model parameters readily identify the physical parameters that will yield that bandwidth. This material can

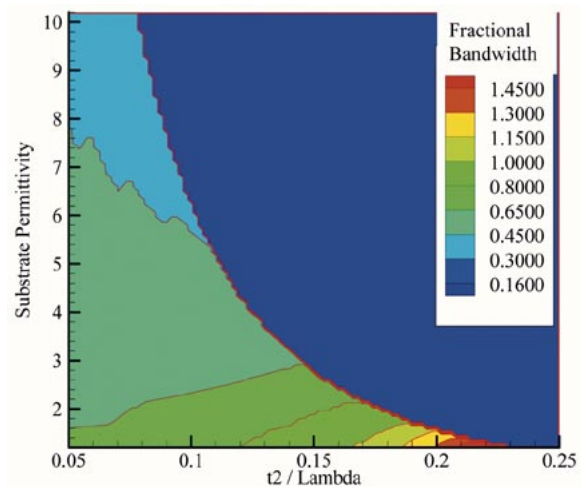


Fig. 18. Contours of total surface wave suppression fractional bandwidth available as a function of substrate thickness and permittivity for a design resonant at 5.5 GHz.

be designed with great flexibility and its applications may vary since it has also been shown that the surface wave suppression band is independent of the  $+/- 90^\circ$  phase band of the reflection coefficient.

## REFERENCES

- [1] D. F. Sievenpiper, "High-impedance electromagnetic surfaces," Ph.D. dissertation, UCLA, 1999.
- [2] V. G. Veselago, "The electrodynamics of substances with simultaneously negative values of  $\epsilon$  and  $\mu$ ," *Soviet Phys. Usp.*, vol. 10, no. 4, pp. 509–514, 1968.
- [3] I. S. Nefedov and S. A. Tretyakov, "Photonic band gap structure containing metamaterial with negative permittivity and permeability," *Phys. Rev. E, Stat. Phys. Plasmas Fluids Relat. Interdiscip. Top.*, vol. 66, p. 036 611, 2002.
- [4] W. M. Merrill, R. E. Diaz, M. LoRe, M. C. Squires, and N. G. Alexopoulos, "Effective medium theories for artificial materials composed of multiple sizes of spherical inclusions in a host continuum," *IEEE Trans. Antennas Propagat.*, vol. 47, pp. 142–148, Jan. 1999.
- [5] W. M. Merrill, S. A. Kyriazidou, and N. G. Alexopoulos, "Is there a relationship between a random and an ordered composite mixture?," *Appl. Comput. Electromagn. Soc. 14th Ann. Rev. Progress*, vol. 1, pp. 151–158, Mar. 1998.
- [6] S. Cohn, "Electrolytic tank measurements for microwave metallic delay-lens media," *JAP*, vol. 21, pp. 674–680, 1950.
- [7] N. Marcuvitz, *Waveguide Handbook*. Stevenage, U.K.: Peregrins, 1986, pp. 218–221.
- [8] J. Brown, "Theory of reflections from the rodged-type artificial dielectric," *The Inst. Elect. Eng.*, pp. 107–115, Nov. 1958.
- [9] R. J. King, D. V. Thiel, and K. S. Park, "The synthesis of surface reactances using an artificial dielectric," *IEEE Trans. Antennas Propagat.*, vol. AP-31, pp. 471–476, May 1983.
- [10] D. Sievenpiper, L. Zhang, R. J. Broas, N. Alexopoulos, and E. Yablonovitch, "High-Impedance electromagnetic surfaces with a forbidden frequency band," *IEEE Trans. Microwave Theory Tech.*, vol. 47, pp. 2059–2074, Nov. 1999.

**Sergio Clavijo** was born in La Paz, Bolivia in 1975. He received the Licenciado in electronic systems from the Military School of Engineering, La Paz, Bolivia and the M.S. in electrical engineering from Arizona State University, Tempe, in 1999 and 2002, respectively, where he is currently pursuing the Ph.D. degree.

His research interests are in electromagnetic theory, high-impedance surfaces and antennas.

**Rodolfo E. Diaz** was born in Santurce, Puerto Rico. He obtained the B.S. degree in physics from Yale University, New Haven, CT, in 1978, the M.S. degree in physics and the Ph.D. degree in electrical engineering from the University of California at Los Angeles, in 1980 and 1992, respectively.

During 20 years in the aerospace industry, his work has spanned many of the disciplines comprising modern electromagnetic engineering. From 1978 to 1983, he was at Rockwell International, Space Division, working on lightning protection, electromagnetic compatibility, and electromagnetic radiation safety on the Space Shuttle. From 1983 to 1988, he worked at Ford Aerospace in the Missile Systems Organization, on the design of novel stripline components, microwave lenses, high temperature broad-band radomes, and absorber materials for broad-band antennas. In 1988, he joined Hexcel Corporation's Advanced Products Division, subsequently acquired in 1995 by Northrop Grumman Corporation, where he led the design, evaluation, and prototyping of electromagnetic composite materials for low observable applications. Currently, he is an Associate Professor in the Department of Electrical Engineering at Arizona State University, Tempe, where he manages the Laboratory for Material-Wave Interactions. He holds 15 patents ranging from the design of broad-band radomes to the amplification of magnetic fields.

**William E. McKinzie III** received the B.S.E.E. degree from the University of Missouri, Rolla, in 1982, and the M.S.E.E. and Ph.D. degrees from the University of California, Los Angeles (UCLA), in 1989 and 1992, respectively.

From 1982 to 1986, he was an RF Circuit Designer at Motorola GEG, Scottsdale, AZ. He worked as a Graduate Research Assistant in the Electrical Engineering Department at UCLA from 1987 through 1992. In 1992, he joined the B2 Division of Northrop Grumman Corporation in Pico Rivera, CA, where he was a Principal Investigator for a variety of antenna related IR&D activities, and supported many other aircraft related antenna projects. In 1996, he joined Atlantic Aerospace Electronics Corporation where he managed several tunable antenna R&D projects. In 2000, he co-founded Etenna Corporation, Laurel, MD, where he now serves as Chief Engineer. His current research interests include the design and low-cost manufacturing of new periodic structures such as artificial magnetic conductors for applications in low profile antennas and antenna isolation treatments.

Dr. McKinzie was awarded the Chancellor's Fellowship to pursue graduate studies at UCLA in 1986. He received an IEEE MTT Society Fellowship in 1989–1990, and was named Outstanding Ph.D. Graduate Student in 1992 from the School of Engineering and Applied Science, UCLA. He was also co-recipient of the IEEE S. E. Schelkunoff Prize Best Paper Award in 1998.